

Anomalous Double-Mode RR Lyrae Stars in the Magellanic Clouds

I. Soszyński^{1*}, R. Smolec², W. A. Dziembowski^{1,2}, A. Udalski¹, M. K. Szymański¹,
L. Wyrzykowski¹, K. Ulaczyk³, R. Poleski^{1,4}, P. Pietrukowicz¹, S. Kozłowski¹,
D. Skowron¹, J. Skowron¹, P. Mróz¹, & M. Pawlak¹

¹ *Warsaw University Observatory, Al. Ujazdowskie 4, 00-478 Warszawa, Poland*

² *Nicolaus Copernicus Astronomical Center, Polish Academy of Sciences, ul. Bartycka 18, 00-716 Warszawa, Poland*

³ *Department of Physics, University of Warwick, Gibbet Hill Road, Coventry, CV4 7AL, UK*

⁴ *Department of Astronomy, Ohio State University, 140 W. 18th Ave., Columbus, OH 43210, USA*

Accepted . Received ; in original form

ABSTRACT

We report the discovery of a new subclass of double-mode RR Lyrae stars in the Large and Small Magellanic Clouds. The sample of 22 pulsating stars have been extracted from the latest edition of the OGLE collection of RR Lyrae variables in the Magellanic System. The stars pulsating simultaneously in the fundamental (F) and first-overtone (1O) modes have distinctly different properties than regular double-mode RR Lyrae variables (RRd stars). The P_{1O}/P_F period ratios of our anomalous RRd stars are within a range 0.725–0.738, while “classical” double-mode RR Lyrae variables have period ratios in the range 0.742–0.748. In contrast to the typical RRd stars, in the majority of the anomalous pulsators the F-mode amplitudes are higher than the 1O-mode amplitudes. The light curves associated with the F-mode in the anomalous RRd stars show different morphology than the light curves of, both, regular RRd stars and single-mode RRab stars. Most of the anomalous double-mode stars show long-term modulations of the amplitudes (Blazhko-like effect). Translating the period ratios into the abundance parameter, Z , we find for our stars $Z \in (0.002, 0.005)$ – an order of magnitude higher values than typical for RR Lyrae stars. The mass range of the RRd stars inferred from the W_I vs. P_F diagram is $(0.55 - 0.75) M_\odot$. These parameters cannot be accounted for with single star evolution assuming a Reimers-like mass loss. Much greater mass loss caused by interaction with other stars is postulated. We blame the peculiar pulsation properties of our stars to the parametric resonance instability of the 1O-mode to excitation of the F- and 2O-modes as with the inferred parameters of the stars $2\omega_{1O} \approx \omega_F + \omega_{2O}$.

Key words: stars: variables: RR Lyrae – stars: oscillations (including pulsations) – Magellanic Clouds

1 INTRODUCTION

The first RR Lyrae star pulsating simultaneously in two radial modes (an RRd star) – AQ Leonis – was identified by Jerzykiewicz & Wenzel (1977). For years, RRd stars have been considered as pure radial pulsators, with no peculiar behaviors like non-radial oscillations or Blazhko effect. This simple picture has changed in recent years with the advent of space-based and massive ground-based photometry. Observations from the space telescopes – MOST,

CoRoT, and Kepler (e.g. Gruberbauer et al. 2007; Chadid 2012; Molnár et al. 2015, respectively) – led to the discovery of additional non-radial modes in RRd variables. Similar detections were also done in the ground-based photometry (Netzel, Smolec & Moskalik 2015; Jurcsik et al. 2015). See Kurtz et al. (2016) for the most recent summary (their table 4) and Dziembowski (2016) for the theoretical model explaining the excitation of non-radial modes in RR Lyrae stars.

Nowadays, the number of known RRd stars reaches several thousands and most of them have been discovered in the time-series photometric databases obtained by the Op-

* E-mail: soszynsk@astrouw.edu.pl

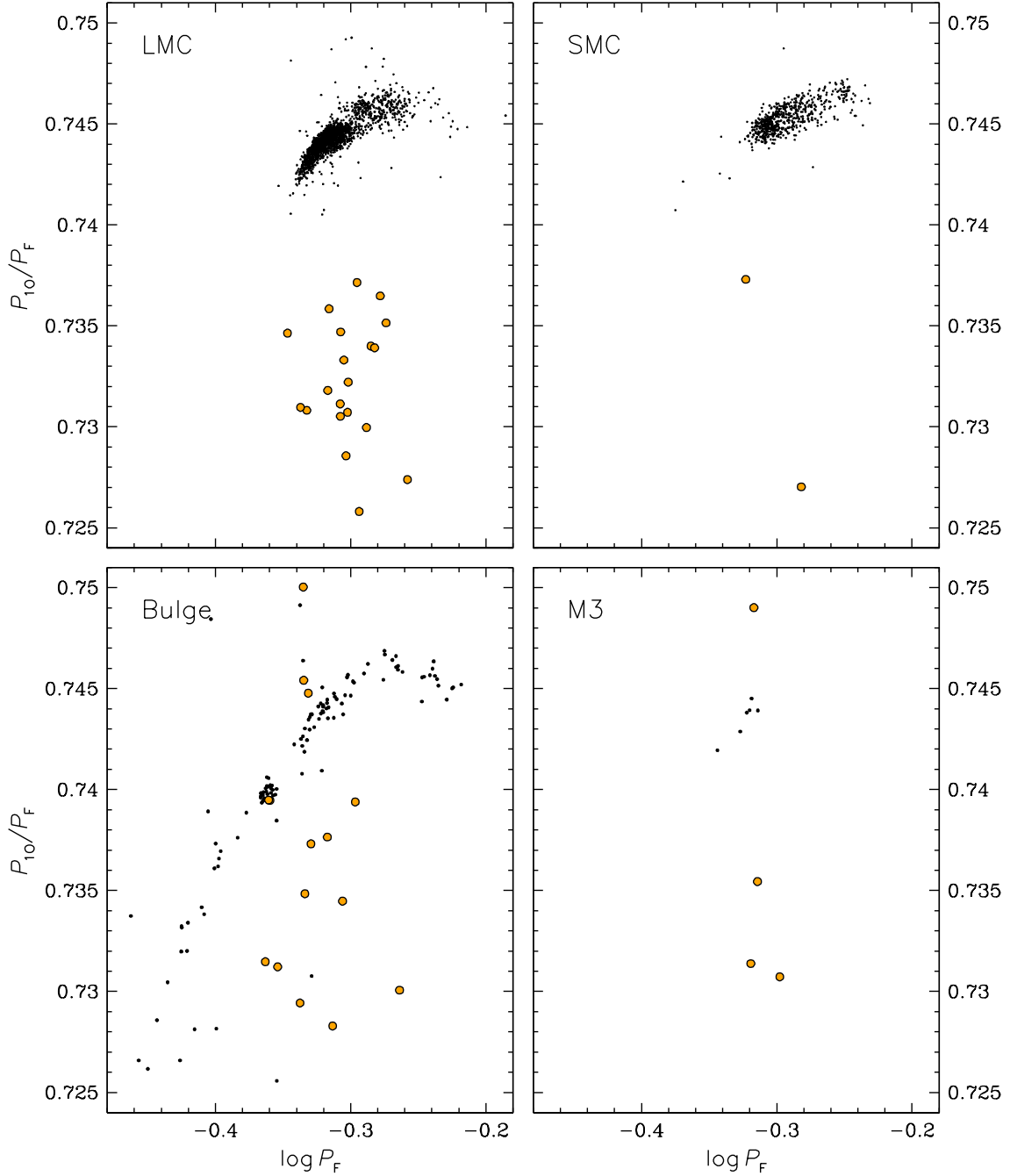


Figure 1. Petersen diagrams for RRd stars in four different stellar systems: LMC, SMC (Soszyński et al. 2014), Galactic bulge (Soszyński et al. 2014; Smolec et al. 2015), and globular cluster M3 (Jurcsik et al. 2014, 2015). Small black dots mark the “classical” RRd stars, large yellow circles mark the anomalous RRd stars in the Magellanic Clouds or Blazhko RRd stars in the Galactic bulge and M3.

tical Gravitational Lensing Experiment (OGLE). The Large (LMC) and Small Magellanic Clouds (SMC) host particularly rich populations of double-mode RR Lyrae stars. The latest release of the OGLE Collection of Variable Stars (Soszyński et al. 2016) contains in total 2624 double-mode RR Lyrae stars in the Magellanic Clouds. RRd stars constitute about 5% and 10% of all RR Lyrae variables in the LMC and SMC, respectively. In turn, in the central regions of the Milky Way the rate of double-mode RR Lyrae is below 0.5% of the entire sample (Soszyński et al. 2011, 2014).

Double-mode RR Lyrae variables occupy a limited region in the Petersen diagram in which the ratios of the first-overtone to fundamental-mode periods (P_{10}/P_F) are plotted against the logarithm of the fundamental-mode period (P_F). In Fig. 1 we present Petersen diagrams for RRd stars in four environments: LMC, SMC (Soszyński et al. 2016), Galactic bulge (Soszyński et al. 2014), and globular cluster M3 (Jurcsik et al. 2014, 2015). Most of the RRd stars form a curved sequence continuing over a narrow range of period ratios $0.742 < P_{10}/P_F < 0.748$. The only known exception

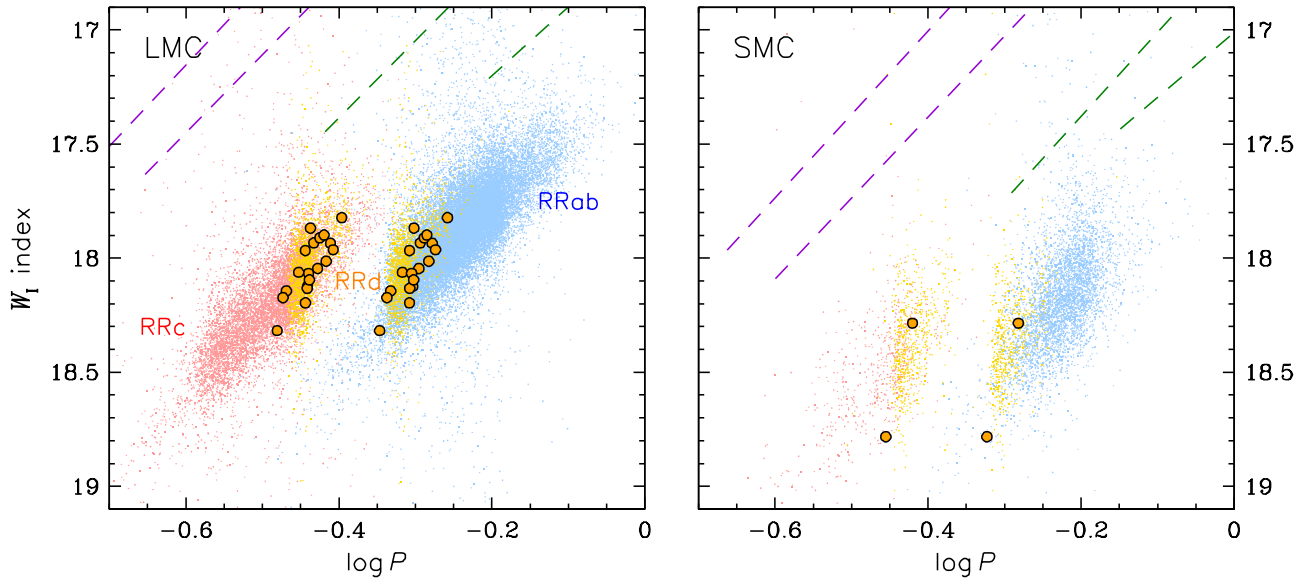


Figure 2. Period–luminosity diagrams for RR Lyrae stars in the LMC (left panel) and SMC (right panel). Blue, red, and yellow dots mark RRab, RRc, and classical RRd stars, respectively. Large circles mark the anomalous RRd stars. Purple and green dashed lines indicate the fits the period–luminosity relations for classical Cepheids (first-overtone and second-overtone modes) and anomalous Cepheids (fundamental and first-overtone modes).

to this rule is the Galactic bulge, where RRd variables form a sequence reaching the period ratios as small as 0.726, which can be explained by a high metal abundance in these stars (Soszyński et al. 2011).

In many environments, a number of double-mode RR Lyrae stars lies below or above the curved sequence in the Petersen diagram. The first RRd stars showing the Blazhko effect (quasi-periodic modulations of pulsation amplitudes and/or phases) were found just among these outliers in the Galactic bulge (Soszyński et al. 2014; Smolec et al. 2015). The same feature was discovered by Jurcsik et al. (2014) for four RRd stars in the globular cluster M3. It seems that Blazhko RRd stars avoid the sequence delineated by regular RRd variables in the Petersen diagram (bottom panels of Fig. 1).

In this paper, we report the discovery of a group of 22 double-mode RR Lyrae stars in the Magellanic Cloud. Our variables have period ratios within the range $0.725 < P_{10}/P_F < 0.738$ – considerably lower than observed in the “classical” RRd stars in these galaxies. We show that both classes of double-mode pulsators present distinct features, like amplitude ratios, shapes of the light curves, presence of the Blazhko effect, and the spatial distribution on the sky. We call the newly identified variables “anomalous RRd stars”.

2 SELECTION OF ANOMALOUS RRD STARS

The sample of anomalous RRd stars has been extracted from the OGLE collection of 45 451 RR Lyrae variables in the Magellanic Clouds (Soszyński et al. 2016). Each light curve was searched for secondary periodicities and, as a result, more than 2600 “classical” RRd stars have been identified. Moreover, five RR Lyrae stars with superimposed eclipsing variability and a number of other multi-periodic variables

were found. In the latter group we noticed 22 (20 in the LMC and 2 in the SMC) double-mode RR Lyrae stars located just below “classical” RRd stars in the Petersen diagram (Fig. 1, top panels). With the longer periods ranged between 0.45 d and 0.55 d and the period ratios between 0.725 and 0.738, these stars distinctly cluster in this region of the Petersen diagram, but they do not form a continuous structure with typical RRd stars.

In the first place, we ensured that our nonstandard double-periodic variables are RR Lyrae stars. Among radially pulsating stars in the Magellanic Clouds, double- or triple-mode classical Cepheids may have periods around 0.5 d (e.g. Soszyński et al. 2015b), but generally they are brighter than RR Lyrae stars with the same periods. Anomalous Cepheids are fainter than classical Cepheids (Soszyński et al. 2015a), but these stars are exclusively single-mode pulsators. In Fig. 2, we plot period–luminosity diagram (where as a luminosity we use the extinction-independent Wesenheit index, defined as $W_I = I - 1.55(V - I)$), for RR Lyrae stars in the LMC and SMC. Both modes of the anomalous double-mode variables are overplotted with large yellow circles. Also the fits to the period–luminosity relations for classical and anomalous Cepheids are displayed in Fig. 2. One can see that our double-mode stars lie exactly on the period–luminosity relations followed by fundamental-mode (RRab) and first-overtone (RRc) RR Lyrae stars. Classical and anomalous Cepheids are much brighter than RR Lyrae stars with the same periods. The $(V - I)$ colours of our variables are practically the same as for typical RRd stars (Fig. 3). Only one star in the LMC is highly reddened by the interstellar extinction and one object in the SMC seems to be slightly bluer and fainter than typical double-mode RR Lyrae stars, but still in the range occupied by RR Lyrae stars. We conclude that our targets must be RR Lyrae stars or, at least, are photometrically indistinguishable from RR Lyrae stars. The positions of these ob-

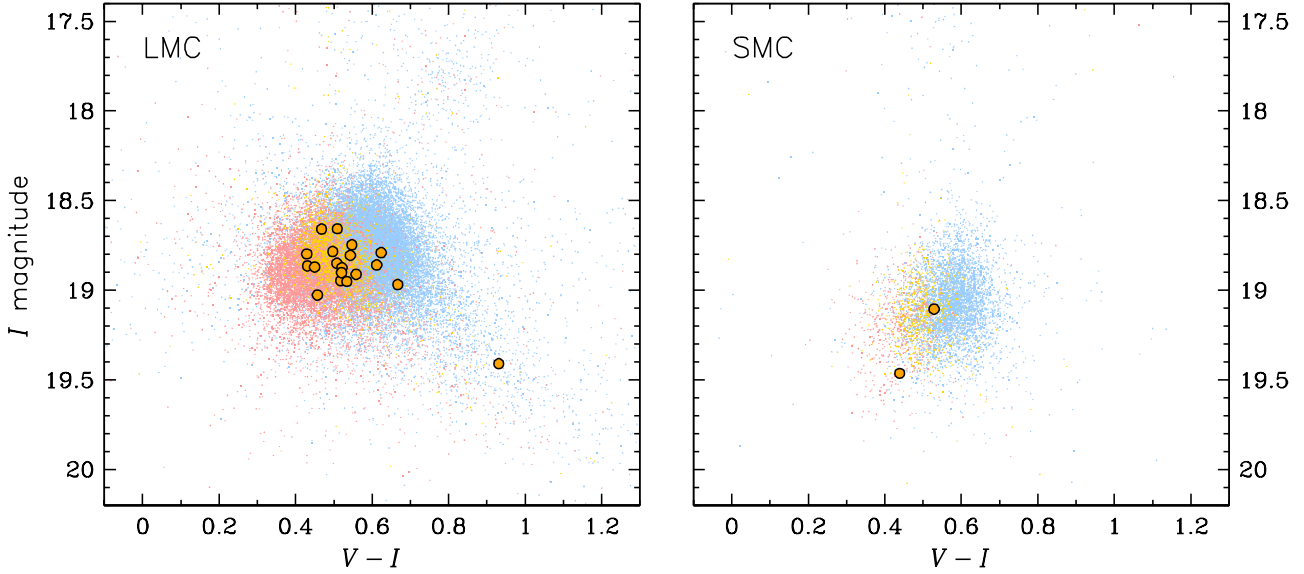


Figure 3. Colour-magnitude diagrams for RR Lyrae stars in the Magellanic Clouds. The colour symbols are the same as in Fig. 2.

jects in the period-luminosity diagram show that they have fundamental and first-overtone radial modes simultaneously excited.

Positions of our anomalous RRd stars in the sky are presented in Fig. 4. For comparison, in the bottom panels we plot the distributions of metal poor ($[\text{Fe}/\text{H}] < -1.8$) and metal rich ($[\text{Fe}/\text{H}] > -0.7$) R Rab stars. The metallicities were derived using the photometric method developed by Jurcsik & Kovács (1996) and calibrated to the I band by Smolec (2005). The anomalous RRd stars tend to cluster towards the center of the LMC, confirming their genuine LMC membership and indicating likely higher metallicity and younger population (see later in the Discussion). We note that metallicity determination for anomalous RRd stars using the Jurcsik & Kovács (1996) method is not possible, due to the anomalous shape of the light curves, as we describe in more detail below.

3 PROPERTIES OF ANOMALOUS RRd STARS

The basic properties of the anomalous RRd stars are collected in Tab. 1. These are: periods of the two pulsation modes, period ratio, amplitude of the fundamental mode, amplitude ratio, and mean I and V band magnitudes. The complete solution of the light curve decomposition is provided in the Appendix available in the on-line version of the journal. Tables A1-A22 contain identifications of all detected frequencies, their values, amplitudes and phases, all with standard errors. Because the vast majority of the OGLE observations have been obtained in the I photometric band, our analysis is based on the light curves in this passband. Between March 2010 and July 2015 OGLE collected from about 200 to nearly 750 I -band data points per star. A median uncertainty of individual photometric measurements for stars as faint as RR Lyrae variables in the Magellanic Clouds is about 0.04 mag.

Anomalous RRd stars differ from normal RRd variables

not only by the P_{10}/P_F period ratios. The first striking difference is the amplitude ratios of both modes. In the bulk of typical RRd stars, the first overtone is the dominant pulsation mode. In anomalous RRd stars in the Magellanic Clouds, the fundamental mode has larger amplitude than the overtone mode in all but three variables.

Moreover, anomalous RRd stars exhibit distinct features of the light curves morphology. Fig. 5 displays light curves of five variables. For each star we present the two modes, prewhitened for the other mode. The first-overtone components have nearly sinusoidal shapes, while the fundamental-mode light curves are usually asymmetric, but they are significantly different than their single-mode counterparts (RRab stars). It can be quantitatively shown using the coefficients of the Fourier light curve decomposition of the form:

$$I(t) = A_0 + \sum_{i=1}^N A_i \cos(i\omega t + \phi_i),$$

where $I(t)$ is the observed I -band magnitude at time t , $\omega = 2\pi/P$ is the angular frequency, P is the pulsation period in days, A_i and ϕ_i represent the amplitude and phase-shift for i th-order respectively, and N is the optimum order of the fit adopted individually for each light curve. The most telling is the period- ϕ_{21} diagram ($\phi_{21} = \phi_2 - 2\phi_1$), which we present in the top panels of Fig. 6. The Fourier phases for the fundamental mode variation in anomalous RRd stars are systematically lower than in both RRab and classical RRd stars. The amplitude ratios, $R_{21} = A_2/A_1$ (bottom panels of Fig. 6), on the other hand, cover a wide range and can exceed the typical values observed in RRab and classical RRd stars, a manifestation of the peculiar light curve shape, with pronounced bump often present at the minimum brightness (Fig. 5). Similar analysis is not possible for the first overtone, as only in a few cases the harmonic is significant.

Another difference is the presence of a modulation of pulsation (the Blazhko effect). Modulation of pulsation amplitude and/or phase manifests through the presence of

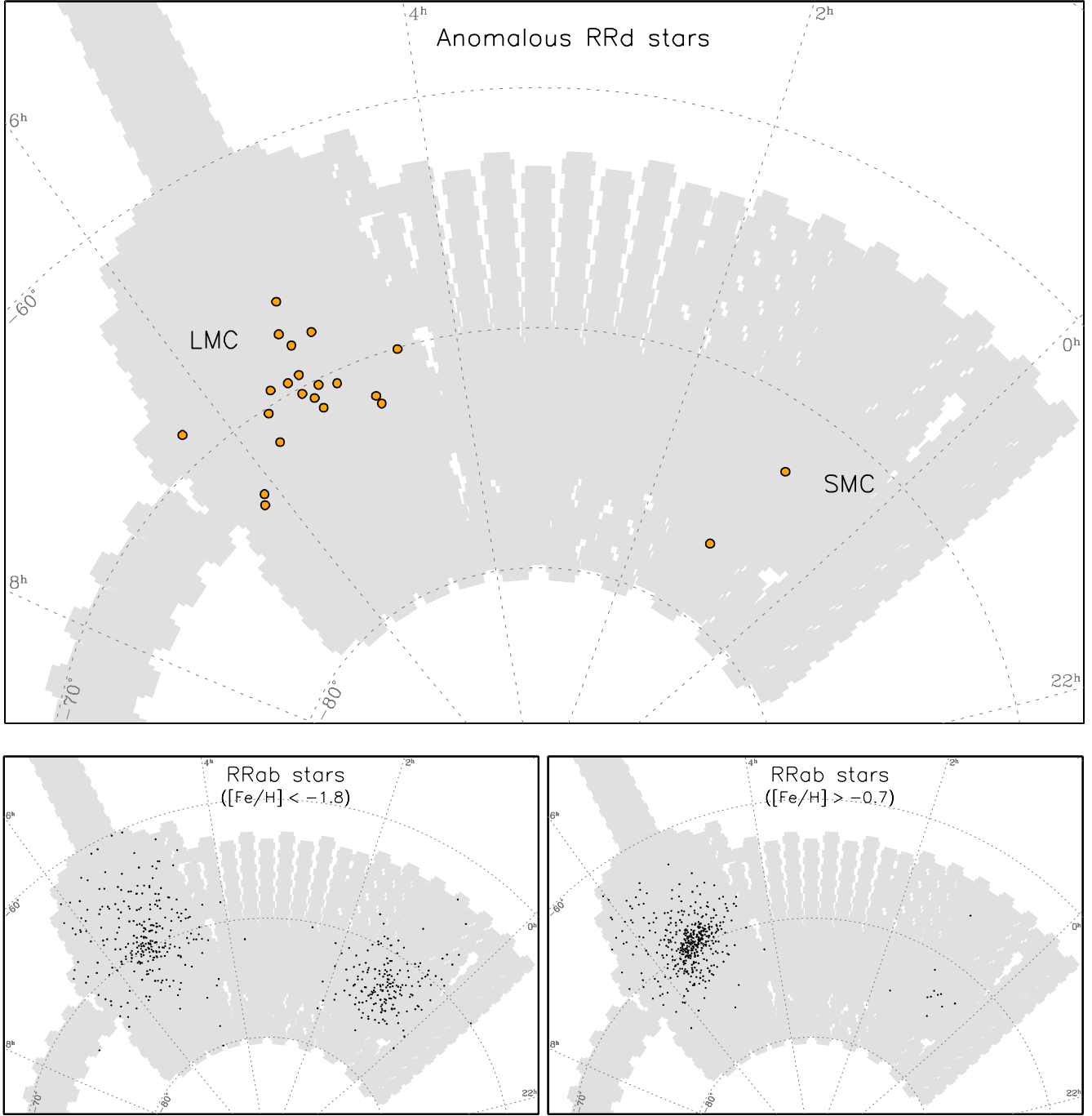


Figure 4. Spatial distribution of RR Lyrae stars in the Magellanic System. Upper panel shows the positions of anomalous RRd stars in the sky. In the bottom panels distributions of metal poor ($[\text{Fe}/\text{H}] < -1.8$) and metal rich ($[\text{Fe}/\text{H}] > -0.7$) RRab stars are presented. Gray area shows the sky coverage of the OGLE fields.

equidistant multiplet structures in the frequency spectrum, centred on the radial mode frequency. Frequency separation within the multiplet corresponds to the modulation frequency, ν_m , and its inverse corresponds to the modulation period. The modulation properties of anomalous RRd stars, determined from the analysis of their frequency spectra, are summarised in Tab. 2, in which we list which radial mode is modulated, provide the modulation period, and modulation amplitudes of both modes. Modulation amplitude is defined as the ratio of the amplitude of the highest side

peak at radial mode frequency to the amplitude of the radial mode. The last column of Tab. 2 lists all detected modulation side peaks. Signature of modulation is detected in 18 out of 22 anomalous RRd stars. Only in six stars we detect equidistant triplet, however. In the majority of cases, only one side peak is detected, which is also interpreted as due to modulation. The modulation multiplets may be highly asymmetric, provided amplitude and phase modulation are of comparable strength and are shifted in phase by $\approx \pm\pi/2$ (Benkő, Szabó & Paparó 2011). Interestingly, at

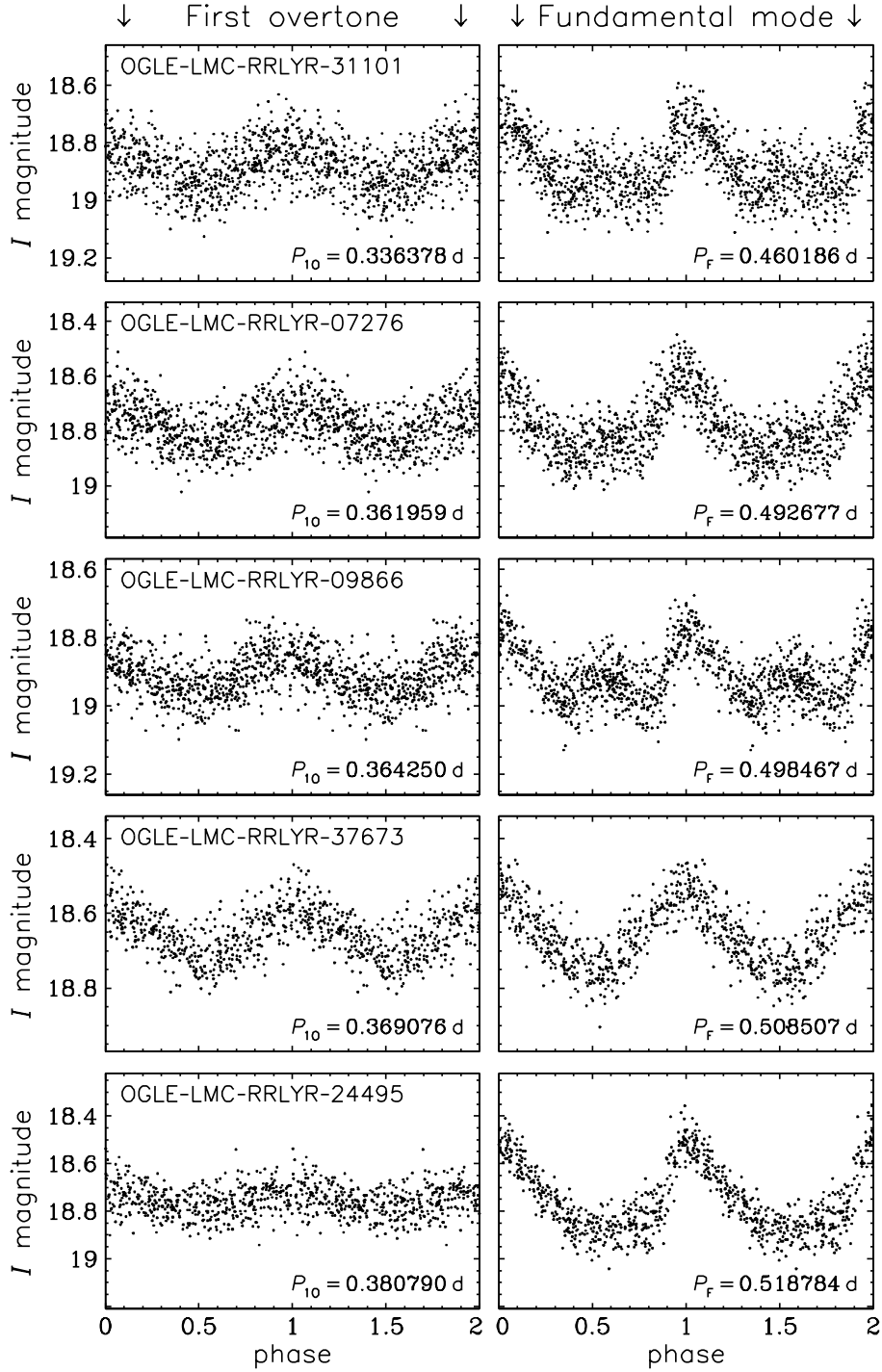


Figure 5. Light curves for a sample of anomalous RRd stars decomposed into the first overtone (left panels) and fundamental mode (right panels) variations.

the frequency of the fundamental mode, it is the lower frequency side peak that is nearly always the higher one (for stars with triplet structure) or it is the only modulation side peak that is detected. The only exception is OGLE-LMC-RRLYR-08917 which we discuss in more detail below. We also note that the amplitude of the modulation of the fundamental mode is typically very high. In two cases (OGLE-LMC-RRLYR-00013 and OGLE-LMC-RRLYR-22167) the low-frequency modulation side peak, $\nu_F - \nu_m$ is slightly

higher than the peak at the fundamental mode frequency, ν_F (Tab. 2). In fact, other interpretation of the close peaks detected in the vicinity of the fundamental mode is possible. The highest peak, of lower frequency, may correspond to the fundamental mode ($\nu_F - \nu_m = \nu'_F$) and the other peak may correspond to the modulation side peak ($\nu_F = \nu'_F + \nu_m$). Such solution seems less reasonable, however, at least in the case of OGLE-LMC-RRLYR-22167, as instead of symmetric

Table 1. Basic properties of anomalous RRd stars: star's ID, 1O and F mode periods, P_{1O}/P_F period ratio, Fourier amplitude of the fundamental mode and A_{1O}/A_F amplitude ratio, mean I - and V -band magnitudes.

Star's ID	P_{1O} (d)	P_F (d)	P_{1O}/P_F	A_F (mag)	A_{1O}/A_F	$\langle I \rangle$ (mag)	$\langle V \rangle$ (mag)
OGLE-LMC-RRLYR-00013	0.363332	0.495475	0.7333	0.088	0.68	18.874	19.395
OGLE-LMC-RRLYR-03878	0.391356	0.532351	0.7351	0.061	1.11	18.805	19.348
OGLE-LMC-RRLYR-04176	0.373427	0.506581	0.7372	0.149	0.25	18.910	19.468
OGLE-LMC-RRLYR-07276	0.361959	0.492677	0.7347	0.111	0.54	18.797	19.226
OGLE-LMC-RRLYR-08767	0.383104	0.522000	0.7339	0.104	0.58	18.784	19.281
OGLE-LMC-RRLYR-08917	0.362271	0.497235	0.7286	0.089	0.65	18.951	19.485
OGLE-LMC-RRLYR-09866	0.364250	0.498467	0.7307	0.063	0.87	18.901	19.421
OGLE-LMC-RRLYR-10802	0.365461	0.499116	0.7322	0.089	0.18	18.657	19.166
OGLE-LMC-RRLYR-12487	0.330622	0.450038	0.7347	0.165	0.27	19.026	19.483
OGLE-LMC-RRLYR-14584	0.355491	0.483089	0.7359	0.160	0.36	19.147	–
OGLE-LMC-RRLYR-19077	0.359980	0.492359	0.7311	0.076	0.78	18.864	19.295
OGLE-LMC-RRLYR-21363	0.359766	0.492473	0.7305	0.044	2.14	19.409	20.340
OGLE-LMC-RRLYR-22167	0.375823	0.514847	0.7300	0.051	1.49	18.859	19.471
OGLE-LMC-RRLYR-24495	0.380790	0.518784	0.7340	0.169	0.19	18.746	19.293
OGLE-LMC-RRLYR-27200	0.401566	0.552068	0.7274	0.105	0.23	18.790	19.414
OGLE-LMC-RRLYR-27329	0.388186	0.527078	0.7365	0.097	0.63	18.968	19.635
OGLE-LMC-RRLYR-30248	0.339935	0.465144	0.7308	0.143	0.22	18.947	19.465
OGLE-LMC-RRLYR-31101	0.336378	0.460186	0.7310	0.096	0.71	18.870	19.320
OGLE-LMC-RRLYR-37673	0.369076	0.508507	0.7258	0.103	0.64	18.659	19.127
OGLE-LMC-RRLYR-38132	0.352750	0.482028	0.7318	0.093	0.89	18.849	19.357
OGLE-SMC-RRLYR-1125	0.350540	0.475437	0.7373	0.166	0.29	19.463	19.902
OGLE-SMC-RRLYR-4726	0.379910	0.522562	0.7270	0.188	0.18	19.105	19.634

Table 2. Modulation properties of the anomalous RRd stars: star's ID, which mode is modulated, modulation period, modulation amplitude and list of all modulation side peaks detected in the frequency spectrum (bold face font indicates the highest side peak at radial mode frequency, asterisk indicates remnant power after the prewhitening and question mark indicates weak detection with $3.0 < S/N < 4.0$).

Star's ID	mode	P_m (d)	$A_m(F)$ (mag)	$A_m(1O)$ (mag)	detected modulation components
OGLE-LMC-RRLYR-00013	F/1O	123.8(3)	1.05	0.49	$\nu_F - \nu_m, \nu_{1O} - \nu_m$
OGLE-LMC-RRLYR-03878	F	201.5(9)	0.95		$\nu_F - \nu_m$
OGLE-LMC-RRLYR-04176	F	19.72(1)	0.26		$\nu_F - \nu_m$
OGLE-LMC-RRLYR-07276	F	44.91(4)	0.52		$\nu_F - \nu_m^*, \nu_F + \nu_m, \nu_F + \nu_{1O} - \nu_m, \nu_F + \nu_{1O} + \nu_m$
OGLE-LMC-RRLYR-08767	F	223.4(1.3)	0.46		$\nu_F - \nu_m$
OGLE-LMC-RRLYR-08917	F/1O	163.8(2)	0.64	1.24	$\nu_F + 2\nu_m, 2\nu_F + 2\nu_m, \nu_{1O} - \nu_m, \nu_{1O} + \nu_m, \nu_F + \nu_{1O} - \nu_m, \nu_F + \nu_{1O} + \nu_m$
OGLE-LMC-RRLYR-09866	F	202.3(1.4)	0.81		$\nu_F - \nu_m, \nu_F + \nu_m, \nu_{1O} - \nu_F - \nu_m(?)$
OGLE-LMC-RRLYR-10802	F	51.12(4)	0.67		$\nu_F - \nu_m^*, \nu_m$
OGLE-LMC-RRLYR-12487	F/1O	130.6(6)	0.19	0.44	$\nu_F - \nu_m, \nu_{1O} + \nu_m$
OGLE-LMC-RRLYR-14584	F/1O	204.9(9)	0.35	0.91	$\nu_F - \nu_m, \nu_F + \nu_m, \nu_{1O} + \nu_m$
OGLE-LMC-RRLYR-19077	1O	56.4(1)		0.74	$\nu_{1O} - \nu_m, \nu_F + \nu_{1O} - \nu_m$
OGLE-LMC-RRLYR-22167	F/1O	143.3(3)	1.09	0.21	$\nu_F - \nu_m, \nu_F + \nu_m, \nu_F + \nu_{1O} - \nu_m, \nu_{1O} - \nu_m, \nu_{1O} - 2\nu_m(?)$
OGLE-LMC-RRLYR-24495	F	174.3(8)	0.23		$\nu_F - \nu_m, \nu_F + \nu_{1O} - \nu_m, 2\nu_F + \nu_{1O} - \nu_m, 3\nu_F + \nu_{1O} - \nu_m$
OGLE-LMC-RRLYR-27200	F	201.7(7)	0.52		$\nu_F - \nu_m, \nu_F + \nu_m(?)$
OGLE-LMC-RRLYR-27329	F	44.86(9)	0.42		$\nu_F - \nu_m^*$
OGLE-LMC-RRLYR-31101	F/1O	206.2(7)	0.60	0.45	$\nu_F - \nu_m^*, \nu_{1O} - 2\nu_m$
OGLE-SMC-RRLYR-1125	F	74.5(4)	0.19		$\nu_F - \nu_m$
OGLE-SMC-RRLYR-4726	F	144.5(1.3)	0.35		$\nu_F - \nu_m$

triplet centered at ν_F (see last column of Tab. 2), asymmetric quintuplet appears at ν_F' .

Modulation periods in the anomalous RRd stars are in the $\sim 20 - 220$ d range. In 11 stars only the fundamental mode is modulated. In one star the first overtone is the only modulated mode and in the remaining six stars both radial modes are modulated with the common period. The only exceptions are OGLE-LMC-RRLYR-08917 and OGLE-LMC-RRLYR-31101.

In OGLE-LMC-RRLYR-31101, at the frequency of the first overtone, we detect only one side peak at $\nu_{1O} - 2\nu_m$. Two interpretations are possible. Either we detect an incomplete quintuplet structure, or first overtone is modulated with period twice as short as the fundamental mode.

OGLE-LMC-RRLYR-08917 is even more intriguing; the most reliable interpretation of the detected modulation side peaks is presented in the last column of Tab. 2. The equidistant modulation triplets are centred at ν_{1O} and at the com-

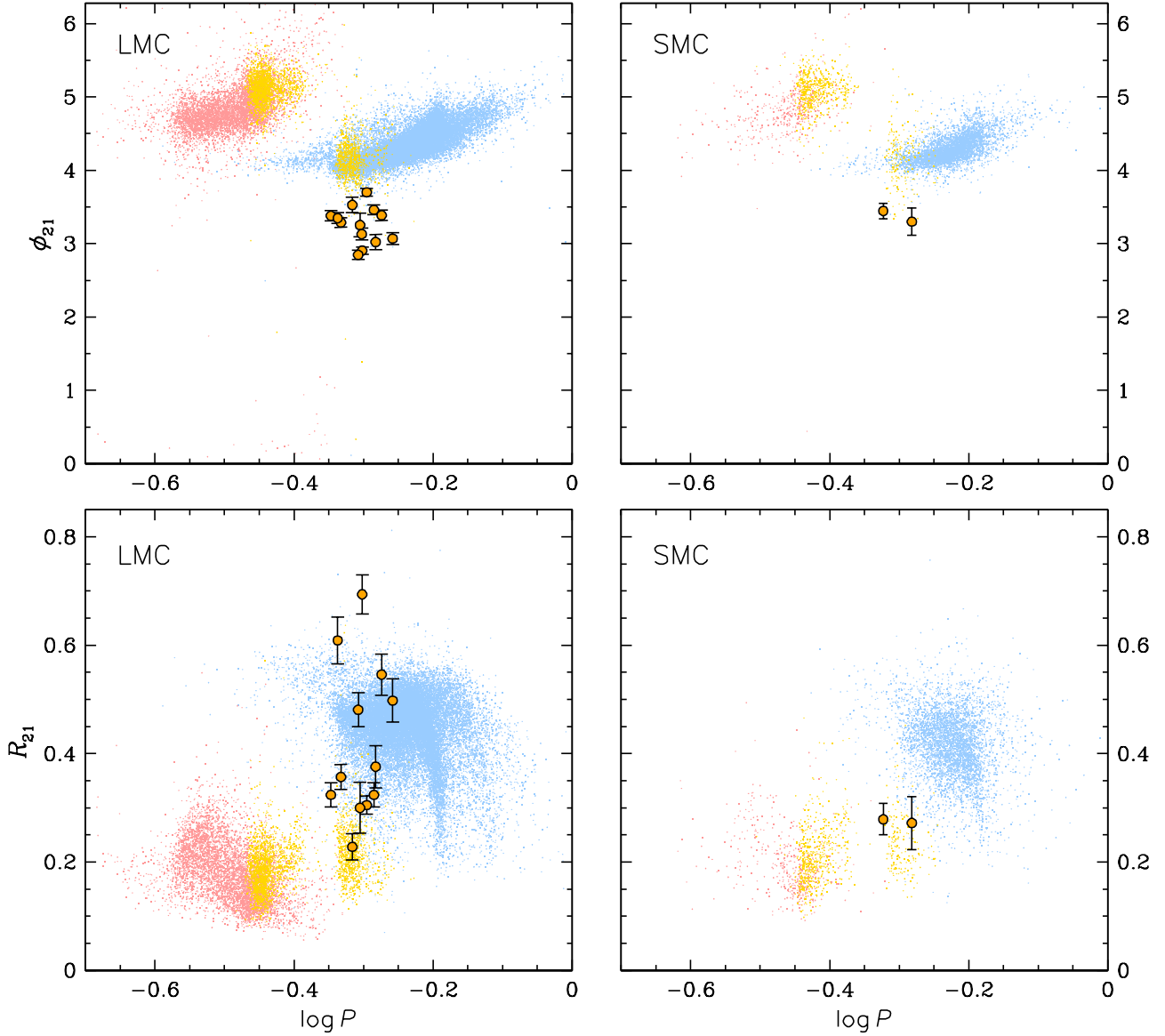


Figure 6. Fourier coefficients, ϕ_{21} vs. $\log P$ (top panels) and R_{21} vs. $\log P$ (bottom panels) for RR Lyrae stars in the Magellanic system. Symbols are the same as in Fig. 2.

bination frequency, $\nu_{10} + \nu_F$. Then, the only side peak at ν_F is located at $\nu_F + 2\nu_m$ indicating that fundamental mode is modulated with period twice as short as the first overtone.

In some cases, after the prewhitening, remnant unresolved power is present at the modulation side peaks (marked with asterisk in the last column of Tab. 2). It indicates that the modulations are irregular.

4 NATURE AND CAUSE OF THE ANOMALOUS RRD PULSATION

To get more insight into the nature of anomalous RRD stars we have computed a grid of linear pulsation models. We used a hybrid of our Warsaw codes: the updated version of the Dziembowski (1977) code and the codes by Smolec & Moskalik (2008). With the former code, very precise computation of mode periods, including non-radial

modes, is possible, but, since convection is treated in the frozen-in approximation, the models do not predict the red edge of the instability strip (IS). This is possible with the latter code, which implements the convection model by Kuhfuß (1986). The two codes use exactly the same OPAL (Iglesias & Rogers 1996) opacity tables and adopt a solar mixture as in Asplund et al. (2009). The two codes were calibrated to produce the same location of the blue edge of the IS in the HR diagram by suitable adjustment of the mixing-length parameter in the Dziembowski's (1977) code. We use unfitted envelope models. We focus on the more numerous LMC sample of anomalous RRD stars. For a given model, mean colours and Wesenheit index were computed through interpolation in the Kurucz (2005)¹ atmosphere

¹ <http://kurucz.harvard.edu/>

models and adopting a 18.5 mag distance modulus to the LMC (Pietrzyński et al. 2013).

The model lines presented in Fig. 7 correspond to the blue and red edge of the classical IS. For a given mass, these were delineated through scan in the model’s absolute luminosity, to fully cover the range of periods observed in anomalous RRd stars.

The comparison of model lines with the observational points in the $(\log P_F, W_I)$ diagrams in the top panels of Fig. 7 shows, almost independently of Z adopted in the models, that masses of the anomalous RRd are spread in the $(0.55 - 0.75)M_\odot$ range. On the other hand the comparison in the Petersen diagrams in the bottom panels of Fig. 7 shows, almost independently of M adopted in the models, that metallicities of the anomalous RRd stars spread in the $\sim (0.002 - 0.005)$ range ($[\text{Fe}/\text{H}] \in (-1.0, -0.5)$). It is essential to note that period–luminosity diagram and Petersen diagram allow us to extract orthogonal information about RRd stars, about their masses and metallicities, respectively.

Pulsation models also provide a hint, what is the cause of anomalous beat pulsation. In Fig. 7, green symbols connected with dotted lines mark the loci of the parametric resonance, $\Delta\omega = 2\omega_{1O} - \omega_F - \omega_{2O} = 0$. It is clear that one can easily adjust M and Z so $\Delta\omega$ is close to zero for the majority of anomalous RRd stars. This suggests that anomalous pulsation form is related to this resonance. A convenient, qualitative analysis of resonant effects is possible thanks to amplitude equations formalism, see Dziembowski (1982), on which we base the below deliberation. Consider an RR Lyrae star evolving redward along the HB and pulsating in the 1O mode. When the amplitude of the relative radius variations, $\epsilon_{1O,2}$, with the harmonic frequency, $2\omega_{1O}$, exceeds certain critical value, ϵ_{crit} , the F and 2O modes become unstable to the parametric excitation. The critical amplitude depends on the distance to resonance center, $\Delta\omega = 2\omega_{1O} - \omega_F - \omega_{2O}$, the linear damping rates, $-\gamma_F$ and $-\gamma_{2O}$, modified by 1O, and the rate of energy transfer from the “mother” mode, 1O, to the two “daughter” modes, F and 2O, which is described by the factor $C_{F,2O}$ in the expression for the critical amplitude (see e.g. Dziembowski 1982):

$$\epsilon_{\text{crit}} \equiv \sqrt{\left[1 + \left(\frac{\Delta\omega}{\gamma_F + \gamma_{2O}}\right)^2\right] \frac{\gamma_F \gamma_{2O}}{|C_{F,2O}|^2}}.$$

During the evolution toward the red edge of the 1O instability range, $|\gamma_F|$ decreases tending to zero, whereas $|\gamma_{2O}|$ increases. With the above expression, we may see that the growing disparity of the damping rates results in widening the frequency range where the parametric excitation takes place.

Smolec & Moskalik (2007, 2010), who studied the finite amplitude development of pulsations in β Cep stars and in classical Cepheids with their nonlinear pulsation code, found that the proximity of the $2\omega_{1O} = \omega_F + \omega_{2O}$ resonance is conducive to F+1O double-mode pulsation. In the frequency spectrum, the 2O mode is hidden due to its low amplitude and the frequency being exactly the same as that of the $2\omega_{1O} - \omega_F$ combination peak, which is a result the phase locking effect.

Blaming the unusual form of pulsation of our anomalous RRd stars to the same resonance may seem strange because the *bona fide* mother mode, first overtone, has nearly always

much lower amplitude in the I band than the F-mode and the signal of its harmonic, which is responsible for the mode coupling, is not (or barely) detectable. However, the high amplitude of the fundamental mode may be explained by its low damping rate. If in the terminal state of the triple-mode pulsation the amplitudes, ϵ , are constant or nearly constant, then

$$E_F \epsilon_F^2 \approx E_{2O} \epsilon_{2O}^2 \approx -\frac{1}{2} E_{1O} \epsilon_{1O}^2,$$

where E is the rate of energy gain (if > 0) or loss (if < 0). These relations follow from the energy balance and from the symmetry of the coupling coefficient, $C_{F,2O}$. Thus, we may have

$$\frac{\epsilon_F}{\epsilon_{1O}} = \sqrt{-\frac{1}{2} \frac{E_{1O}}{E_F}} \gg 1.$$

We also note that amplitude equations for the discussed resonance permit oscillatory solutions around the mean, resonant, triple-mode state. Thus, the resonance is a plausible explanation for the modulation observed in the majority of anomalous RRd stars.

5 DISCUSSION AND CONCLUSIONS

Anomalous RRd stars in the Magellanic Clouds are not the first such objects known in the Universe. A number of double-mode RR Lyrae stars in the Galactic bulge have period ratios below 0.742 (Soszyński et al. 2014), although not all of them are considered anomalous. In the bulge, the sequence followed by classical RRd stars in the Petersen diagram is not truncated at ≈ 0.742 as in the LMC, but continues towards the lower period ratios (bottom left panel of Fig. 1). In addition, there is a group outside of this sequence with distinct features, like the presence of the Blazhko effect (Smolec et al. 2015), peculiar light curve shape, or anomalous amplitude ratio. The same systematic differences show four anomalous RRd stars identified in the globular cluster M3 by Jurcsik et al. (2014, 2015) (bottom right panel of Fig. 1). However, anomalous RRd variables in the Magellanic Clouds constitute the largest sample of such objects known in any stellar system. This is the first time that there is no doubt that anomalous RRd stars are not just extreme cases of “classical” RRd stars, but they represent a separate subclass of double-mode RR Lyrae stars.

Modelling of RR Lyrae stars *ab initio* still represents a considerable challenge. The problem is particularly difficult for the high metallicity objects, such as considered in this paper. At the highest metallicities ($Z = 0.005$), the main sequence evolutionary time for a star arriving at the horizontal branch (HB) with $\sim 0.55 M_\odot$, exceeds the age of the Universe (even assuming large mass loss along the red giant branch, e.g. Pietrinferni et al. 2006; Choi et al. 2016). At the low metallicities ($Z = 0.002$) the stars do not reach the instability strip after helium ignition, becoming red clump objects on the cool side of the classical instability strip. The clear separation of the anomalous RRd stars from the classical RRd sequence in the Petersen diagram (Fig. 1) suggests a different evolution channel towards the instability strip, likely through a stripped red giant phase. We find support for this idea by comparison of the Petersen diagrams for the LMC and the Galactic bulge. We note a strong disparity in

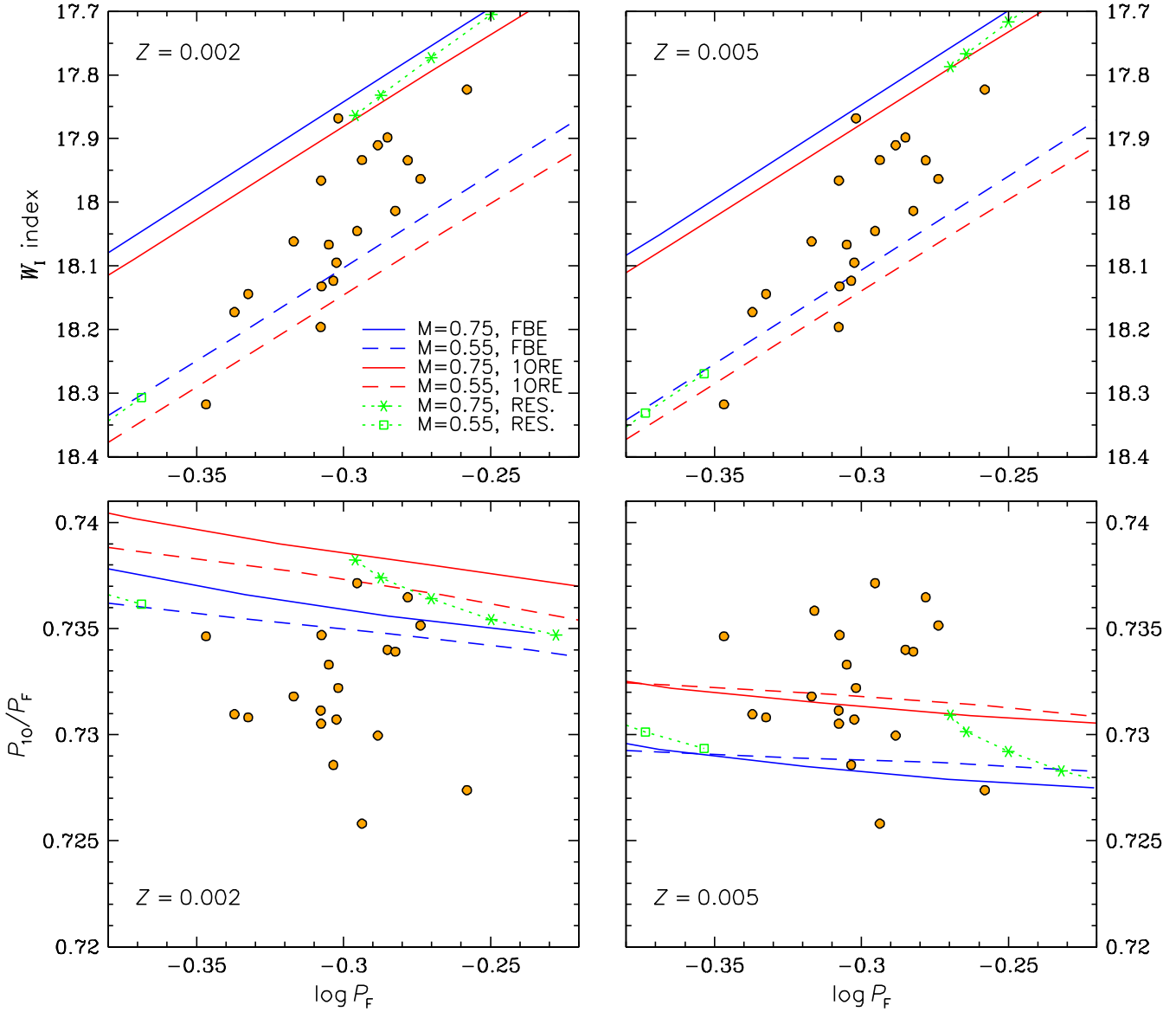


Figure 7. Models in the central part of the instability strip, where the F and IO are simultaneously unstable, are confronted with observations. Red and blue lines connect the corresponding red (IORE) and blue (FBE) edges in the range of L chosen to cover the the range of periods of the anomalous RRd stars. The green lines connect the resonance centers ($\Delta\omega = 0$, RES).

the incidence rate of anomalous RRd stars in these two environments: as compared to classical RRd stars, anomalous variables are about 7 times more numerous in the Galactic bulge than in the LMC. The absence of luminous red giants has been noted in the inner parts of the Galactic bulge (e.g. Bartko et al. 2010; Kieffer & Bogdanović 2016, and references therein). It has been explained as a result of interactions of stars in red giant phase with the accretion disc surrounding the central black hole (Kieffer & Bogdanović 2016). The stripping may also result from star-to-star interactions.

We have pointed in the previous section that the models for anomalous RRd star are close to the parametric resonance, $2\omega_{10} = \omega_F + \omega_{20}$. One of the observed anomalies in the discussed stars is the higher amplitude of the fundamental mode. We have shown, based on the amplitude equa-

tions formalism, that it is possible provided the fundamental mode is weakly damped, but it has to be checked with direct hydrodynamic modelling. Such modelling should also gain more insight into the nature of the pronounced bumps visible near the minima of brightness in some fundamental-mode light curves. Such features may be related to shock phenomena or arise from the resonant mode interaction. We plan to perform the nonlinear modeling with the Warsaw code. The spectroscopic confirmation of high-metallicity of anomalous RRd stars, deduced from pulsation models, is also needed. We note that we cannot base on the photometric method of estimating RR Lyrae stars' metallicity (e.g. Jurcsik & Kovács 1996), as the fundamental mode light curves in anomalous RRd stars have peculiar shape.

ACKNOWLEDGEMENTS

This work has been supported by the Polish Ministry of Science and Higher Education through the program “Ideas Plus” award No. IdP2012 000162. The OGLE project has received funding from the Polish National Science Centre grant MAESTRO no. 2014/14/A/ST9/00121. RS acknowledges support from the Polish National Science Centre grants no. DEC-2012/05/B/ST9/03932 and DEC-2015/17/B/ST9/03421.

REFERENCES

- Asplund M., Grevesse N., Sauval A. J., Scott P., 2009, *ARA&A*, 47, 481
- Bartko H., 2010, *ApJ*, 708, 834
- Benkő J.M., Szabó R., Paparó M., 2011, *MNRAS*, 417, 974
- Chadid M., 2012, *A&A*, 540, A68
- Choi J., Dotter A., Conroy C., Cantiello M., Paxton B., Johnson B.D., 2016, *ApJ*, 823, 102
- Dziembowski W., 1977, *Acta Astron.*, 27, 95
- Dziembowski W., 1982, *Acta Astron.*, 32, 147
- Dziembowski W., 2016, *Comm. Konkoly Obs.*, vol. 105, 23
- Gruberbauer M., et al., 2007, *MNRAS*, 379, 1498
- Iglesias C.A., Rogers F.J., 1996, *ApJ*, 464, 943
- Jerzykiewicz M., Wenzel W., 1977, *Acta Astron.*, 27, 35
- Jurcsik J., Kovács G., 1996, *A&A*, 312, 111
- Jurcsik J., Smitola P., Hajdu G., Nuspl J., 2014, *ApJ*, 797, L3
- Jurcsik J., et al., 2015, *ApJS*, 219, 25
- Kieffer T.F., Bogdanović T., 2016, *ApJ*, 823, 155
- Kuhfuß R., 1986, *A&A*, 160, 116
- Kurtz D.W., et al. 2016, *MNRAS*, 455, 1237
- Kurucz R.L., 2005, *Mem. S.A.It. Suppl.*, 8, 14
- Molnár L., et al. 2015, *MNRAS*, 452, 4283
- Netzel H., Smolec R., Moskalik P., 2015, *MNRAS*, 447, 1173
- Pietrinferni A., Cassisi S., Salaris M., Castelli F., 2006, *ApJ*, 642, 797
- Pietrzyński G., et al., 2013, *Nature*, 495, 76
- Smolec R., 2005, *Acta Astron.*, 55, 59
- Smolec R., Moskalik P., 2007, *MNRAS*, 377, 645
- Smolec R., Moskalik P., 2008, *Acta Astron.*, 58, 193
- Smolec R., Moskalik P., 2010, *A&A*, 524, A40
- Smolec R., et al., 2015, *MNRAS*, 447, 3756
- Soszyński I., et al., 2011, *Acta Astron.*, 61, 1
- Soszyński I., et al., 2014, *Acta Astron.*, 64, 177
- Soszyński I., et al., 2015a, *Acta Astron.*, 65, 233
- Soszyński I., et al., 2015b, *Acta Astron.*, 65, 297
- Soszyński I., et al., 2016, *Acta Astron.*, 66, 131

APPENDIX A: COMPLETE LIGHT-CURVE SOLUTIONS

This paper has been typeset from a \LaTeX file prepared by the author.

Table A1. Light curve solution for OGLE-LMC-RRLYR-00013. The consecutive columns contain frequency id., frequency value, amplitude with standard error, phase with standard error and remarks. Entries are sorted by increasing frequency. In case of frequency values the error of the last two digits of independent frequencies is given in parenthesis. ‘bl’ in the ‘remarks’ column indicates a frequency of the Blazhko modulation in case no significant peak was detected in the frequency spectrum directly at $\nu = \nu_m$. Amplitude and phase are not given then.

freq. id	f [d $^{-1}$]	A [mmag]	σ	ϕ [rad]	σ	remarks
ν_m	0.008077(18)					bl
$\nu_F - \nu_m$	2.010188	91	4	5.93	0.57	
ν_F	2.018264(12)	87	4	3.38	0.46	
$\nu_{1O} - \nu_m$	2.744229	29	4	3.07	0.88	
ν_{1O}	2.752306(21)	59	4	3.96	0.78	
$2\nu_F$	4.036529	28	4	2.33	0.93	

Table A2. Same as Tab. 1 for OGLE-LMC-RRLYR-03878.

freq. id	f [d $^{-1}$]	A [mmag]	σ	ϕ [rad]	σ	remarks
ν_m	0.004964(22)					bl
$\nu_F - \nu_m$	1.873496	59	3	0.81	0.65	
ν_F	1.878460(12)	62	3	5.53	0.46	
ν_{1O}	2.555219(17)	63	3	0.80	0.64	
$2\nu_F$	3.756919	31	3	0.23	0.91	

Table A3. Same as Tab. 1 for OGLE-LMC-RRLYR-04176.

freq. id	f [d $^{-1}$]	A [mmag]	σ	ϕ [rad]	σ	remarks
ν_m	0.05070(3)					bl
$\nu_F - \nu_m$	1.923317	40	4	5.05	1.19	
ν_F	1.974019(8)	152	4	4.20	0.29	
ν_{1O}	2.67790(4)	33	4	3.54	1.48	
$2\nu_F$	3.948039	42	4	4.05	0.58	

Table A4. Same as Tab. 1 for OGLE-LMC-RRLYR-07276.

freq. id	f [d $^{-1}$]	A [mmag]	σ	ϕ [rad]	σ	remarks
ν_m	0.022267(21)					bl
$\nu_F - \nu_m$	2.007461	62	4	1.92	0.72	
ν_F	2.029729(8)	118	4	3.52	0.28	
$\nu_F + \nu_m$	2.051996	23	4	2.72	0.96	
ν_{1O}	2.762746(21)	58	4	3.40	0.79	
$2\nu_F$	4.059457	46	4	2.19	0.58	
$\nu_F + \nu_{1O} - \nu_m$	4.770207	28	4	1.17	1.07	
$\nu_F + \nu_{1O} + \nu_m$	4.814742	7	4	4.98	1.32	
$3\nu_F$	6.089186	20	4	1.80	0.88	

Table A5. Same as Tab. 1 for OGLE-LMC-RRLYR-08767.

freq. id	f [d $^{-1}$]	A [mmag]	σ	ϕ [rad]	σ	remarks
ν_m	0.004477(24)					bl
$\nu_F - \nu_m$	1.911232	49	4	4.77	0.92	
ν_F	1.915709(9)	106	4	3.28	0.33	
ν_{1O}	2.610255(18)	59	4	5.85	0.69	
$2\nu_F$	3.831418	39	4	1.71	0.67	

Table A6. Same as Tab. 1 for OGLE-LMC-RRLYR-08917.

freq. id	f [d ⁻¹]	A [mmag]	σ	ϕ [rad]	σ	remarks
ν_m	0.006103(8)					bl
ν_F	2.011122(11)	85	3	6.12	0.41	
$\nu_F + 2\nu_m$	2.023329	55	3	4.16	0.57	
$\nu_{1O} - \nu_m$	2.754261	69	3	2.90	0.47	
ν_{1O}	2.760365(12)	55	3	1.66	0.44	
$\nu_{1O} + \nu_m$	2.766468	52	3	3.92	0.60	
ν_u	4.02089(7)	18	3	5.98	2.52	
$2\nu_F + 2\nu_m$	4.034452	31	3	5.71	0.77	
$\nu_F + \nu_{1O} - \nu_m$	4.765384	20	3	5.31	0.69	
$\nu_F + \nu_{1O} + \nu_m$	4.777590	17	3	5.10	0.61	

Table A7. Same as Tab. 1 for OGLE-LMC-RRLYR-09866.

freq. id	f [d ⁻¹]	A [mmag]	σ	ϕ [rad]	σ	remarks
ν_m	0.00494(3)					bl
$\nu_{1O} - \nu_F - \nu_m$	0.734274	10	3	0.66	1.83	
$\nu_{1O} - \nu_F$	0.739217	22	3	3.93	1.15	
$\nu_F - \nu_m$	2.001210	53	3	4.54	1.22	
ν_F	2.006152(12)	66	3	3.10	0.45	
$\nu_F + \nu_m$	2.011095	17	3	4.62	1.41	
ν_{1O}	2.745369(27)	50	3	0.74	1.01	
$2\nu_F$	4.012305	58	3	1.33	0.90	

Table A8. Same as Tab. 1 for OGLE-LMC-RRLYR-10802.

freq. id	f [d ⁻¹]	A [mmag]	σ	ϕ [rad]	σ	remarks
ν_m	0.019561(15)	26	3	0.13	0.59	
$\nu_F - \nu_m$	1.983981	60	3	1.42	0.53	
ν_F	2.003543(7)	90	3	1.44	0.25	
ν_{1O}	2.73627(6)	18	3	5.02	2.09	
$2\nu_F$	4.007086	64	3	4.11	0.50	
$3\nu_F$	6.010628	20	3	1.58	0.77	
$4\nu_F$	8.014171	13	3	4.86	0.99	

Table A9. Same as Tab. 1 for OGLE-LMC-RRLYR-12487.

freq. id	f [d ⁻¹]	A [mmag]	σ	ϕ [rad]	σ	remarks
ν_m	0.00765(4)					bl
$\nu_{1O} - \nu_F$	0.802569	20	4	0.89	0.98	
$\nu_F - \nu_m$	2.214378	32	4	0.71	1.36	
ν_F	2.222033(7)	173	4	5.00	0.26	
ν_{1O}	3.024602(24)	50	4	6.16	0.92	
$\nu_{1O} + \nu_m$	3.032257	22	4	1.51	1.48	
$2\nu_F$	4.444067	56	4	5.67	0.53	

Table A10. Same as Tab. 1 for OGLE-LMC-RRLYR-14584.

freq. id	f [d ⁻¹]	A [mmag]	σ	ϕ [rad]	σ	remarks
ν_m	0.004880(20)					bl
ν_u	0.81330(6)	28	5	3.48	2.20	
$\nu_F - \nu_m$	2.065133	54	5	3.42	0.74	
ν_F	2.070013(9)	155	5	5.37	0.34	
$\nu_F + \nu_m$	2.074893	50	5	3.63	0.93	
ν_{1O}	2.81301(3)	51	5	0.74	1.17	
$\nu_{1O} + \nu_m$	2.817892	47	5	6.07	1.16	
$2\nu_F$	4.140025	33	5	6.20	0.68	

Table A11. Same as Tab. 1 for OGLE-LMC-RRLYR-19077.

freq. id	f [d ⁻¹]	A [mmag]	σ	ϕ [rad]	σ	remarks
ν_m	0.01773(3)					bl
ν_F	2.031038(17)	73	4	4.70	0.64	
$\nu_{1O} - \nu_m$	2.760208	44	4	3.01	0.97	
ν_{1O}	2.777934(22)	59	4	2.82	0.83	
$\nu_F + \nu_{1O} - \nu_m$	4.791246	25	4	3.41	1.12	

Table A12. Same as Tab. 1 for OGLE-LMC-RRLYR-21363.

freq. id	f [d ⁻¹]	A [mmag]	σ	ϕ [rad]	σ	remarks
ν_F	2.030567(35)	45	5	1.03	1.34	
ν_{1O}	2.779582(18)	93	5	5.85	0.67	

Table A13. Same as Tab. 1 for OGLE-LMC-RRLYR-22167.

freq. id	f [d ⁻¹]	A [mmag]	σ	ϕ [rad]	σ	remarks
ν_m	0.006980(15)					bl
$\nu_F - \nu_m$	1.935345	58	4	1.48	0.63	
ν_F	1.942325(13)	53	4	1.19	0.50	
$\nu_F + \nu_m$	1.949305	46	4	4.93	0.83	
$\nu_{1O} - 2\nu_m$	2.646871	14	4	4.74	1.16	
$\nu_{1O} - \nu_m$	2.653851	16	4	1.71	0.77	
ν_{1O}	2.660831(16)	74	4	0.01	0.58	
$\nu_F + \nu_{1O} - \nu_m$	4.596176	21	4	3.69	0.87	

Table A14. Same as Tab. 1 for OGLE-LMC-RRLYR-24495.

freq. id	f [d ⁻¹]	A [mmag]	σ	ϕ [rad]	σ	remarks
ν_m	0.005737(27)					bl
$\nu_F - \nu_m$	1.921847	37	4	1.02	0.98	
ν_F	1.927583(5)	167	4	1.44	0.20	
ν_{1O}	2.626123(29)	34	4	2.66	1.09	
$2\nu_F$	3.855167	53	4	4.75	0.40	
$\nu_F + \nu_{1O} - \nu_m$	4.547969	16	4	5.31	1.23	
$3\nu_F$	5.782750	32	4	2.37	0.60	
$2\nu_F + \nu_{1O} - \nu_m$	6.475553	20	4	3.01	1.21	
$4\nu_F$	7.710334	17	4	5.99	0.83	
$3\nu_F + \nu_{1O} - \nu_m$	8.403136	17	4	0.80	1.24	

Table A15. Same as Tab. 1 for OGLE-LMC-RRLYR-27200.

freq. id	f [d ⁻¹]	A [mmag]	σ	ϕ [rad]	σ	remarks
ν_m	0.004957(17)					bl
$\nu_F - \nu_m$	1.806415	54	3	4.63	0.63	
ν_F	1.811372(6)	103	3	1.33	0.22	
$\nu_F + \nu_m$	1.816328	12	3	5.87	0.76	
ν_{1O}	2.49025(4)	21	3	0.50	1.63	
$2\nu_F$	3.622743	51	3	4.22	0.43	
$3\nu_F$	5.434115	15	3	2.39	0.67	

Table A16. Same as Tab. 1 for OGLE-LMC-RRLYR-27329.

freq. id	f [d ⁻¹]	A [mmag]	σ	ϕ [rad]	σ	remarks
ν_m	0.02229(4)					bl
$\nu_F - \nu_m$	1.874958	40	5	4.69	1.55	
ν_F	1.897251(17)	96	5	2.27	0.66	
ν_{1O}	2.576085(28)	59	5	6.23	1.05	

Table A17. Same as Tab. 1 for OGLE-LMC-RRLYR-30248.

freq. id	f [d ⁻¹]	A [mmag]	σ	ϕ [rad]	σ	remarks
ν_F	2.149873(6)	139	4	4.58	0.21	
ν_{1O}	2.94174(4)	34	4	1.10	1.28	
$2\nu_F$	4.299747	51	4	4.56	0.43	
$3\nu_F$	6.449621	22	4	5.28	0.66	
$4\nu_F$	8.599494	20	4	5.39	0.87	

Table A18. Same as Tab. 1 for OGLE-LMC-RRLYR-31101.

freq. id	f [d ⁻¹]	A [mmag]	σ	ϕ [rad]	σ	remarks
ν_m	0.004851(16)					bl
$\nu_F - \nu_m$	2.168182	54	4	3.62	0.63	
ν_F	2.173033(8)	90	4	4.24	0.29	
$\nu_{1O} - 2\nu_m$	2.963147	23	4	4.57	1.37	
ν_{1O}	2.972848(22)	52	4	4.61	0.82	
$2\nu_F$	4.346066	58	4	3.88	0.57	

Table A19. Same as Tab. 1 for OGLE-LMC-RRLYR-37673.

freq. id	f [d ⁻¹]	A [mmag]	σ	ϕ [rad]	σ	remarks
$\nu_{1O} - \nu_F$	0.742925	16	4	5.96	0.87	
ν_F	1.966541(10)	107	4	5.81	0.39	
ν_{1O}	2.709466(19)	61	4	0.09	0.70	
$\nu_F + \nu_{1O}$	4.676008	16	4	1.94	0.79	

Table A20. Same as Tab. 1 for OGLE-LMC-RRLYR-38132.

freq. id	f [d ⁻¹]	A [mmag]	σ	ϕ [rad]	σ	remarks
ν_F	2.074566(19)	95	6	1.60	0.73	
ν_{1O}	2.834866(19)	87	6	3.24	0.77	

Table A21. Same as Tab. 1 for OGLE-SMC-RRLYR-1125.

freq. id	f [d ⁻¹]	A [mmag]	σ	ϕ [rad]	σ	remarks
ν_m	0.01343(7)					bl
$\nu_F - \nu_m$	2.089900	32	6	4.73	2.48	
ν_F	2.103327(10)	166	7	3.02	0.41	
ν_{1O}	2.85274(4)	52	6	4.42	1.46	
$2\nu_F$	4.206654	45	6	1.83	0.82	

Table A22. Same as Tab. 1 for OGLE-SMC-RRLYR-4726.

freq. id	f [d ⁻¹]	A [mmag]	σ	ϕ [rad]	σ	remarks
ν_m	0.00692(6)					bl
$\nu_F - \nu_m$	1.906728	65	9	5.63	2.36	
ν_F	1.913648(18)	185	8	1.51	0.74	
ν_{1O}	2.63220(9)	41	9	1.18	4.01	
$2\nu_F$	3.827297	46	8	4.74	1.49	